

Novel Implicit Lorentz Force-Type Magnetic Bearing for High-Precision Agile Maneuver of Magnetically Suspended Gyrowheel

WANG Qirui*, LIU Qiang, LI Zhuang

College of Mechanical Engineering, Beijing Institute of Petrochemical Technology, Beijing 102617, P.R. China

(Received 25 April 2021; revised 10 June 2021; accepted 15 July 2021)

Abstract: The Lorentz force-type magnetic bearing (LFTMB) with good linearity is suitable for the high-precision deflection control of the magnetically suspended gyrowheel (MSGW). Two kinds of novel implicit LFTMBs are proposed in allusion to the poor magnetic flux density uniformity of the existing explicit LFTMB. The improvement of uniformity is realized under the paramagnetic contribution of magnetic ring. Their structures are introduced, the mathematical models are established based on the equivalent magnetic circuit method and the magnetic fields are analyzed by the finite element method based on the design parameters. Simulation results indicate that the magnetic flux density uniformity of implicit LFTMBs is superior to the traditional explicit LFTMB. Furthermore, the implicit trapezoid LFTMB with double magnetic circuits is better than that of those with single magnetic circuit, in terms of the magnetic flux density uniformity and the magnetic flux density. The magnetic flux density of implicit trapezoid double magnetic circuits LFTMB is verified by the experiment. The error between the experimental results and the simulation results is within 5%, which shows that the implicit trapezoid double magnetic circuits LFTMB is promising to meet the high-precision agile maneuver requirement of the magnetically suspended gyrowheel.

Key words: finite element method; Lorentz force-type magnetic bearing (LFTMB); magnetically suspended gyrowheel (MSGW); magnetic flux density fluctuation

CLC number: V249.1 **Document code:** A **Article ID:** 1005-1120(2021)S-0057-12

0 Introduction

Flywheel is the key inertial actuator used to generate control moment for realizing the attitude stabilization and adjustment of spacecraft^[1]. Compared with conventional mechanical flywheel, magnetically suspended flywheels (MSFWs) have aroused widespread concern owing to their remarkable advantages of no stiction-friction effect, long service life, high control precision and micro vibration and so on^[2]. MSFW is classified as three types according to different rotational speeds of rotors, namely the magnetically suspended reaction flywheel/gyroscope^[3], the magnetic bias of momentum wheel^[4] and the attitude control energy storage

flywheel^[5]. In the above MSFWs, the high-precision control moment is obtained by changing the rotational speed of a rotor. However, the control moment is too small, which is unsatisfactory to realize the urgent requirements of agile maneuver for spacecraft. The magnetically suspended gyrowheel (MSGW) combines the merits of MSFW with high-precision control moment, and outputs the instantaneous large moment by changing the rotor angular momentum direction^[6]. Therefore, MSGW is promising to be the ideal inertial actuator for new spacecraft.

In order to simultaneously satisfy high-precision and large torque, various magnetic suspension schemes applied to MSGW are proposed in Refs.[7-

*Corresponding author, E-mail address: wangqiruibt@163.com.

How to cite this article: WANG Qirui, LIU Qiang, LI Zhuang. Novel implicit Lorentz force-type magnetic bearing for high-precision agile maneuver of magnetically suspended gyrowheel[J]. Transactions of Nanjing University of Aeronautics and Astronautics, 2021, 38(S): 57-68.

<http://dx.doi.org/10.16356/j.1005-1120.2021.S.008>

15]. Murakami et al.^[7] proposed a MSGW with three axis controlled magnetic bearing (MB). The axial translation and radial deflection can be controlled. Seddon and Pechev^[8] presented another active-passive MSGW. The radial deflection and translation were realized by magnetic reluctance MBs, and the axial translation was achieved by passive control. Due to the uncontrollability of the passive MB in Refs.[7-8], Tang et al.^[9] developed a 5-DOF active MSGW whose control precision is improved by magnetic reluctance MBs. However, the control precision is limited due to the nonlinear force generated by magnetic reluctance MBs. As the deflection torque of the Lorentz force-type magnetic bearing (LFTMB) is proportional to the control current, the control precision is superior to that of magnetic reluctance MB^[8-9]. Gerlach et al.^[10] proposed a 5-DOF active scheme that both of the translation and deflection relied on LFTMBs. The rotor rotational inertia is limited due to the low bearing capacity of LFTMB in the pure LFTMBs scheme. Therefore, the researchers turned their attention to the hybrid configuration schemes integrating the advantages of magnetic reluctance MB with high stiffness and LFTMB with high precision. Li et al.^[11] introduced a hybrid scheme based on LFTMB for deflection control, magnetic resistance MBs for active radial translation control and passive axial support. Similar to the schemes in Refs.[7-11], the control precision of the MSGW is reduced on account of the mutual coupling between the active force and the passive force. To remedy the mutual coupling, Xiang and Tang et al.^[12-13] developed a 5-DOF active hybrid MSGW through conical permanent magnet biased MB for radial/axial translation and LFTMB for deflection. The couplings between translation and deflection are eliminated when the rotor is suspended at the equilibrium position. However, when the deflection occurs on rotor, new interference moments are generated due to the change in the shape of the conical/cylinder air gap. Damien et al.^[14] presented a spherical suspension and support MSGW to improve the control precision, taking the advantage of constant spherical air gap. On the basis of Refs.[12-14], Liu et al.^[15] presented another

MSGW with the spherical air gap further to realize the requirements of high-precision control. The interference moments eliminated in the air gap shape is constant during rotor deflecting.

Above all, the existing LFTMBs in Refs.[10-15] have explicit structures that magnetic steels are located on both sides of the air gap. The magnetic flux density uniformity in the air gap is poor on account of the magnetic flux leakage at the end of magnetic poles. In this paper, two implicit LFTMB schemes are proposed in view of the nonuniform magnetic flux density of the explicit LFTMB. The LFTMB deflection model is established, and the relationship between the deflection torque and the uniformity of the magnetic flux density is obtained. Then, the finite element model is built for contrastive analysis among the three schemes. Analysis results show that the scheme of implicit trapezoid double magnetic circuits LFTMB has better magnetic flux density uniformity. A LFTMB prototype based on the optimal scheme is developed, and the magnetic flux density experiments are performed to verify its effectiveness and validity.

1 LFTMB Schemes in MSGW

1.1 MSGW structure and its working principle

The configuration of the MSGW is shown in Fig.1. The MSGW is mainly composed of the motor, sensors, spherical rotor with rated speed of 9 000 r/min and angular momentum of 15 N·m·s, axial/radial spherical MBs providing translation force and LFTMB producing deflection torque.

The radial spherical MBs are composed of eight magnetic poles to realize rotor translation in the X and Y directions, respectively. The magnetic circuits of radial spherical MBs are shown in thick solid lines. The axial spherical MB consists of a pair of magnetic pole to realize the translation control in the Z direction. The magnetic circuits generated by the axial MBs are shown in thin solid line. The 2-DOF rotor deflections are achieved by LFTMB, and its circuit is shown in thin dash lines. In Ref.[15], there are introductions in detail of the MSGW structure and working principle. The deflection

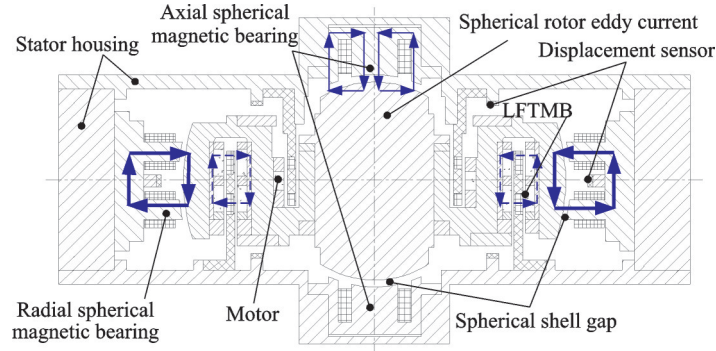


Fig.1 Configuration of MSGW

torque of the MSGW is provided by LFTMB which rotates the rotor along the X/Y axes by a reaction force. Therefore, the magnitude and accuracy of the MSGW output control moment are directly determined by the LFTMB performance.

1.2 Mathematical model of deflection in MSGW

The structure of LFTMB is shown in Fig. 2, which is composed of four permanent rings, two pairs of coils, two magnetic rings, magnetic isolation rings and stator frame. The four permanent magnetic rings (PMRs) are at the end of magnetic poles. Magnetic circuit indicated in solid line is generated by PMR via PMR, air gap, coils and magnet flux ring. The magnetic rings of the same layer are magnetized in the same direction, which generates a

stable magnetic field between the inner and outer magnet rings. To close the magnetic circuit, the upper and the lower magnetic rings are opposite in magnetization direction. Two pairs of coils wound on the stator frame are used in series. When the turns of the two pairs of coils are the same, the ampere forces generated by the current in different directions in the same magnetic field are in the same magnitude and in opposite directions. The deflection torque generated by LFTMB is linear with the current. Therefore, the output deflection torque of the MSGW has the merit of high precision. Taking the scheme in Fig.2 as an example, the influencing factors on the magnitude and precision of the output deflection torque are analyzed by building a mathematical model.

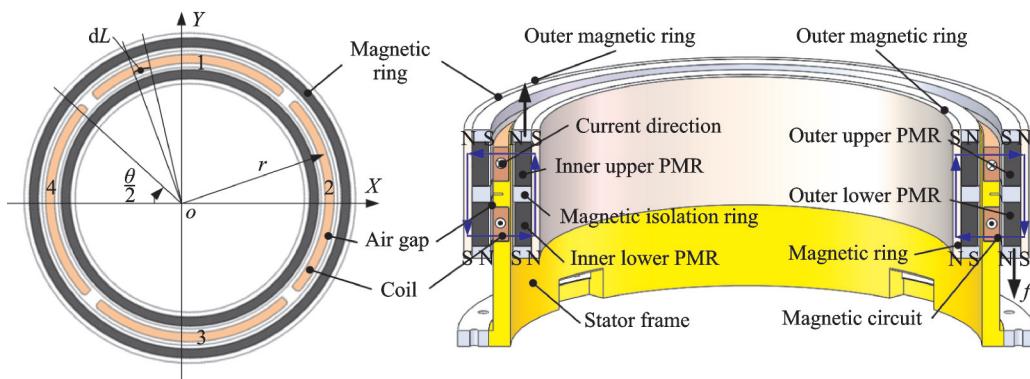


Fig.2 Schematic diagram of LFTMB structure

As shown in Fig.2, the $OXYZ$ coordinate system is established with the geometric center of the LFTMB stator as the center of the circle. The four sets (two pairs) of coils with the same angle around the circumferential direction are defined as θ . When the micro element dL is selected in the circumferential direction, the ampere force of the coil can be expressed by

pressed by

$$df_i = NBI_i dL \quad (1)$$

where $i=1, 2, 3, 4$; N is the number of turns of the coil, I the excitation current, B the magnetic flux density of air gap at the coil position, and L the circumferential length of a coil. The mathematical expression of L is $x^2 + y^2 = r^2$. Here r is the radius for

the position where the coil is located. dL is obtained by curvilinear integral for a length. Then T is calculated by integral for dT as follows

$$T_i = 2 \int_0^{\frac{\theta}{2}} NBI_i r dy = 2NBI_i r^2 \cos \frac{\theta}{2} \quad (2)$$

The deflection torques around the X and Y directions are expressed respectively as

$$\begin{cases} T_x = 4NB(I_{y-} + I_{y+})r^2 \cos \frac{\theta}{2} \\ T_y = 4NB(I_{x-} + I_{x+})r^2 \cos \frac{\theta}{2} \end{cases} \quad (3)$$

To calculate the torsional stiffness, the excitation current of Y channel coil is separately considered ($I_{x-} = I_{x+} = 0$), $I_{y-} = I_{y+} = I_t$ in deflection control. Then T_x in Eq.(4) can be expressed as

$$T_x = 8NB r^2 \cos \frac{\theta}{2} I_t = K_{it} I_t \quad (4)$$

where K_{it} is the torsional current stiffness. It can be obtained when I_t is taken the partial derivative by T_x and I_t is 0 from Eq.(4). It can be seen from Eq.(4) that the control precision of output moment is related to K_{it} . The more stable K_{it} is, the higher control precision is. Nevertheless, K_{it} is related to B . The more uniform B is, the more stable K_{it} is. However, B is not evenly distributed in reality. Improving the magnetic flux density uniformity of LFTMB is the key mean to improve the precision of output moment of the MSGW.

1.3 LFTMB schemes

1.3.1 Explicit LFTMB

The explicit LFTMB^[7-15] scheme is shown in Fig.2. The PMRs are located on both sides of the air gap, and the closed magnetic fluxes produced by four PMRs flow across four evenly distributed coils through two magnetic rings. Based on the structure, the equivalent magnetic circuit is shown in Fig.3 in the case of the magnetic flux leakage at the end of magnetic poles. The F_{pmai} is the magnetomotive force of the PMR ($i=1,2,3,4$), and R_{pmai} the magnetic reluctance corresponding to F_{pmai} . Φ_u and Φ_c are the main magnetic fluxes passing through the upper and lower windings, respectively. Φ_{su} and Φ_{sc} are the magnetic flux leakages which is not passing through the upper and lower windings, respectively. R_u , R_{su} , R_c , and R_{sc} are the magnetic resistances corresponding to Φ . R_i and R_o are the magnetic reluctance of the inner and outer magnetic rings, re-

spectively. R_{si} and R_{so} are the magnetic resistances of magnetic flux leakage, respectively. The magnetic flux Φ can be expressed as

$$\Phi = \begin{bmatrix} \Phi_{su} \\ \Phi_u \\ \Phi_{sc} \\ \Phi_c \end{bmatrix} = \begin{bmatrix} R_u / (R_{su} + R_u) \\ R_{su} / (R_{su} + R_u) \\ R_c / (R_{sc} + R_c) \\ R_{sc} / (R_{sc} + R_c) \end{bmatrix} \Phi_m \quad (5)$$

where Φ_m is main magnetic flux corresponding to the main magnetic circuit between permanent rings. As the magnetic reluctance of magnetic ring is far smaller than that of air gap and PMR, magnetic reluctance of R_i / R_{si} and R_o / R_{so} can be ignored in Fig.3. Moreover, the four PMRs are the same, and then the corresponding magnetic flux density B can be obtained as

$$B = [B_{su} \ B_u \ B_{sc} \ B_c]^T = \text{diag}(A_{su}, A_u, A_{sc}, A_c)^{-1} \Phi = \text{diag}(A_{su}, A_u, A_{sc}, A_c)^{-1} \cdot \begin{bmatrix} R_u / (R_{su} + R_u) \\ R_{su} / (R_{su} + R_u) \\ R_c / (R_{sc} + R_c) \\ R_{sc} / (R_{sc} + R_c) \end{bmatrix} \cdot \frac{4H_c l_{pma}}{4R_{pma} + \frac{R_u R_{su}}{R_u + R_{su}} + \frac{R_c R_{sc}}{R_c + R_{sc}}} \quad (6)$$

where H_c is coercivity, l_{pa} the corresponding magnetization length, B_{su} , B_u , B_{sc} , and B_c are the corresponding magnetic flux density to the Φ_{su} , Φ_u , Φ_{sc} and Φ_c , respectively. A_{su} , A_u , A_{sc} , and A_c are the corresponding equivalent sectional areas to the Φ_{su} , Φ_u , Φ_{sc} and Φ_c , respectively.

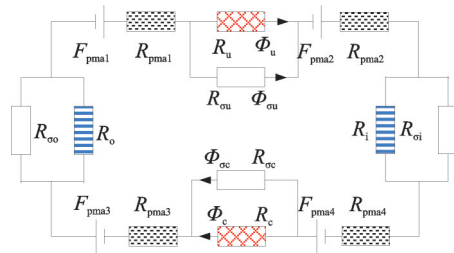


Fig.3 Equivalent magnetic circuit of explicit LFTMB

The finite element method is used to analyze the LFTMB. The finite element model is shown in Fig.4(a). There is serious magnetic flux leakage and axial fluctuation at the edge of rectangular PMRs, and the magnetic flux density reduction caused by magnetic flux leakage is shown in orange in Fig.4(b). Furthermore, the PMRs are spliced

with several evenly distributed arc PMRs due to the difficulty in processing. The splicing gap causes seri-

ous circumferential magnetic flux density fluctuation shown in ellipse of Fig.4(b).

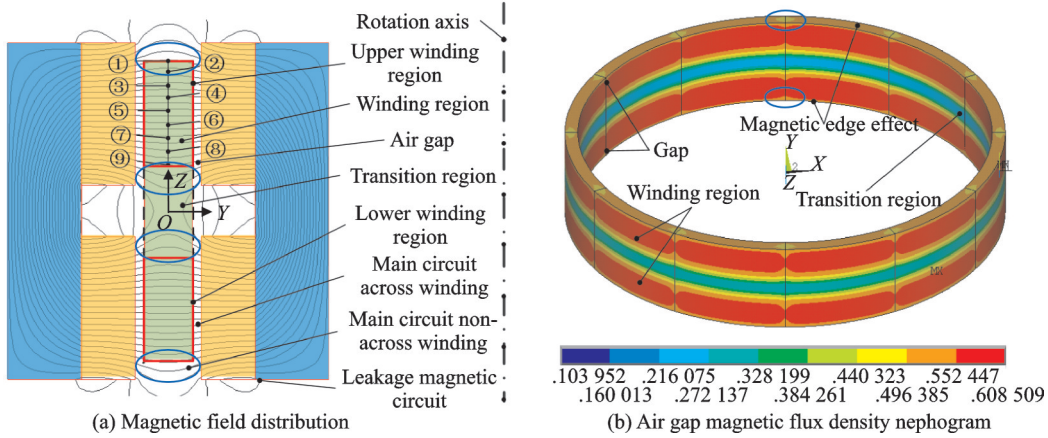


Fig.4 Explicit LFTMB

The air gap magnetic flux density in the cross section is shown in Fig.5(a). Magnetic flux distribution along the radial direction is antisymmetric. It can be seen from Fig.5(a) that the air gap magnetic flux density in the middle of air gap is the smallest along Y direction and the largest along Z direction in winding regions. The maximum and minimum magnetic flux densities are 0.594 T and 0.446 T, respectively, and the corresponding magnetic flux density fluctuation along radial direction is 25%. As shown in Fig.4(a), the nine circles along Z direction in center winding region are se-

lected. The magnetic flux density in nine circles is calculated by finite element method, and the magnetic flux density curves are drawn in Fig.5(b). According to the analysis results above, there are fluctuations of circumferential magnetic flux density in the spliced air gaps, which is in great agreement with the turning points on the nine curves in Fig.5 (b). The maximum magnetic flux density with 0.575 T is in the 5th line, and its minimum with 0.425 T is in the 1st line. The circumferential magnetic flux density fluctuation in the winding region is 26%.

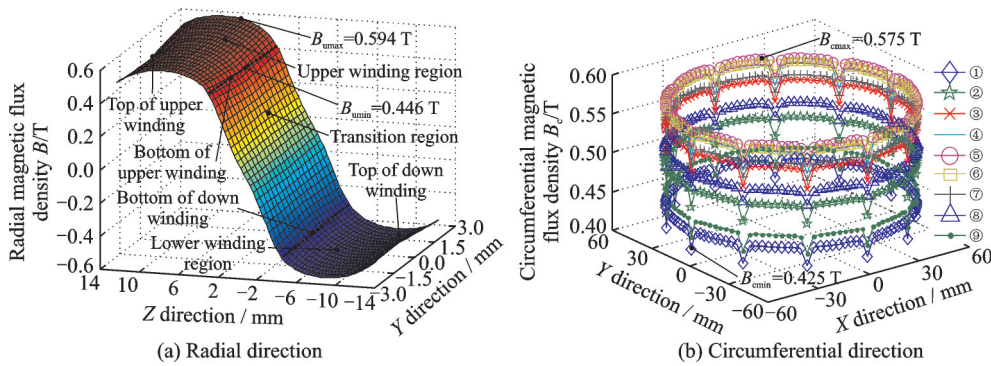


Fig.5 Magnetic flux density distribution

1. 3. 2 Implicit single magnetic circuit LFTMB

The implicit single magnetic circuit LFTMB scheme is shown in Fig.6(a). The PMR embedded in the magnetic ring is the essential difference between implicit single magnetic circuit LFTMB and explicit LFTMB. Confirmed by finite element analy-

sis in Fig.7, circumferential magnetic flux density fluctuation in explicit scheme is eliminated under paramagnetic contribution of magnetic ring. The equivalent magnetic circuit is shown in Fig.6(b).

The parameters in the equivalent magnetic circuit shown in Fig.6 (b) are similar as those in the

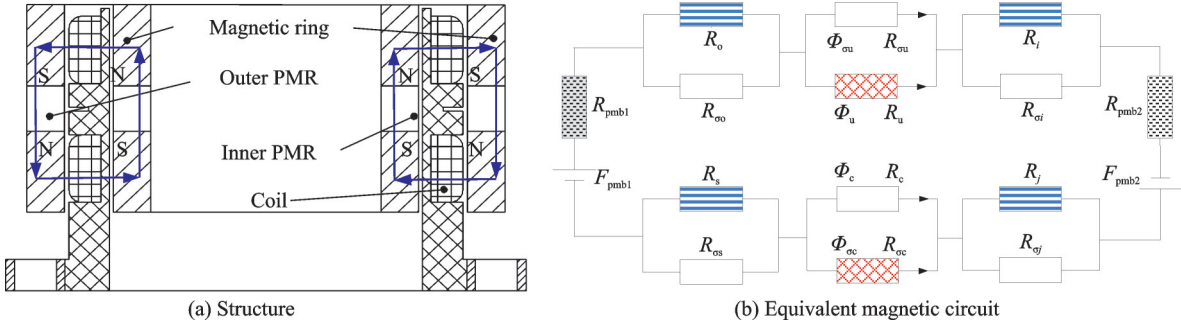


Fig.6 Implicit single magnetic circuit LFTMB

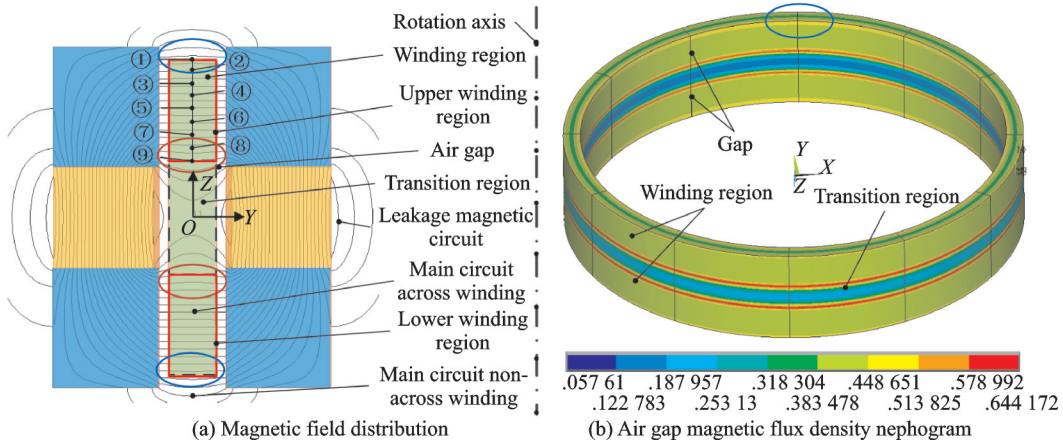


Fig.7 Implicit single magnetic circuit LFTMB density nephogram

scheme of explicit LFTMB. The added R_i and R_j are the magnetic reluctance of magnetic rings. R_{σ_i} and R_{σ_j} are the magnetic reluctance corresponding to magnetic flux leakage, respectively. The magnetic reluctance of $R_i//R_{\sigma_i}$, $R_o//R_{\sigma_o}$, $R_o//R_{\sigma_o}$ and $R_o//$

$$B = \text{diag}(A_{\sigma_u}, A_u, A_{\sigma_c}, A_c)^{-1} \begin{bmatrix} R_u/(R_{\sigma_u} + R_u) \\ R_{\sigma_u}/(R_{\sigma_u} + R_u) \\ R_c/(R_{\sigma_c} + R_c) \\ R_{\sigma_c}/(R_{\sigma_c} + R_c) \end{bmatrix} \cdot \frac{2H_c l_{\text{pmb}}}{2R_{\text{pmb}} + \frac{R_u R_{\sigma_u}}{R_u + R_{\sigma_u}} + \frac{R_c R_{\sigma_c}}{R_c + R_{\sigma_c}}} \quad (7)$$

The finite element model is shown in Fig.7. In order to more accurately evaluate the performance of LFMBs for high-precision agile maneuver of magnetically suspended gyrowheel, the section thickness and width of the winding are consistent with the overall dimensions of explicit LFTMB, and the same in the analysis of implicit trapezoid double magnetic circuits LFTMB. It can be seen that the magnetic flux distribution of implicit single magnetic circuit LFTMB is much better than that of explicit scheme. There is hardly circumferential magnetic flux fluctuation caused by spliced air gap in Fig.7

R_{σ_o} can also be ignored. In addition, the two PMRs are the same, and the corresponding magnetization length is l_{pmb} . The magnetic flux density B can be expressed as follows

(b). Similarly, there is still some magnetic flux density nonuniformity induced by the magnetic flux leakage at the end of magnetic poles in Fig.7(a). However, due to the magnetic flux leakage of the rectangular PMRs embedded in the magnetic rings, the magnetic flux density in the interface between the winding and transition regions is maximum. And it is shown in red in Fig.7(b). The radial magnetic flux distribution in winding region is described in Fig.8(a). The maximum and minimum magnetic flux densities of implicit single magnetic circuit LFTMB are 0.428 T and 0.397 T, respectively.

The magnetic flux density fluctuation along the radial direction of implicit single magnetic circuit LFT-MB with 7.2% is obviously better than that of explicit LFTMB with 25%. The circumferential magnetic flux distribution is analyzed by the nine circles which are selected in Fig.7(a). Its distribution is

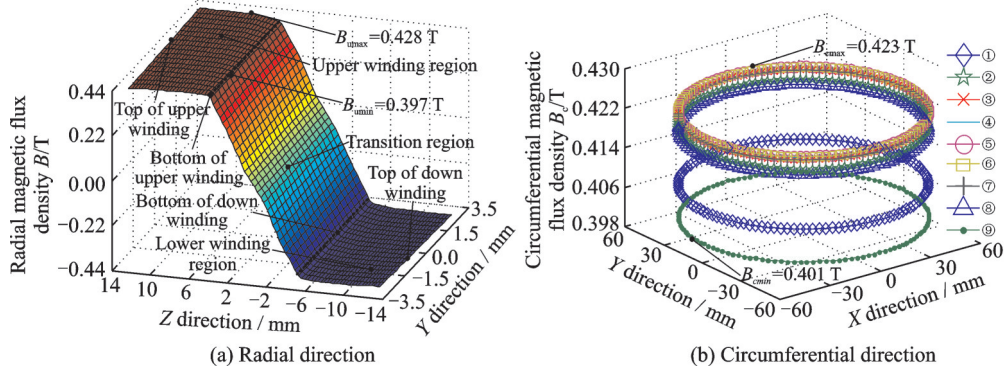
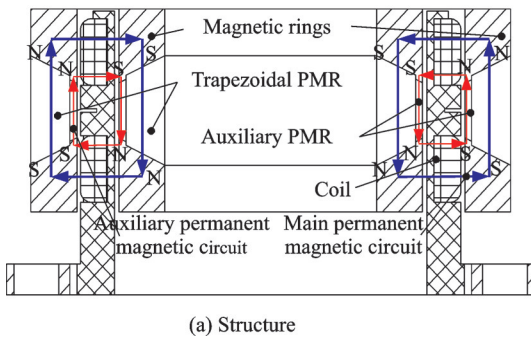


Fig.8 Magnetic flux density distribution

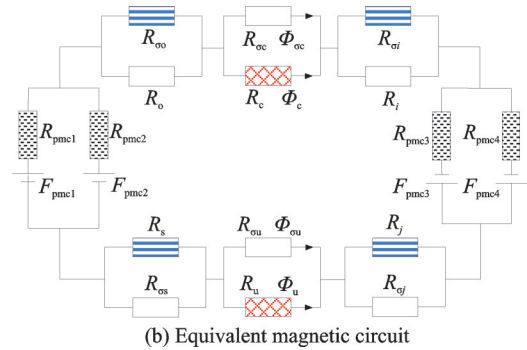
1.3.3 Implicit trapezoid double magnetic circuits LFTMB

The implicit trapezoid double magnetic circuits LFTMB scheme is shown in Fig.9(a). There are two closed magnetic flux circuits supplied by main and auxiliary PMRs in implicit trapezoid double magnetic circuits LFTMB scheme. Both main and auxiliary PMRs are all with trapezoidal section. The roles of trapezoidal and auxiliary

shown in Fig.8(b). The maximum and minimum magnetic flux densities are 0.423 T in the 5th line and 0.401 T in the 9th line, respectively. Its corresponding circumferential magnetic flux density fluctuation is 5.2%, far less than that of explicit LFT-MB with 26%.



(a) Structure



(b) Equivalent magnetic circuit

Fig.9 Implicit trapezoid double magnetic circuits LFTMB

The parameters are consistent with the former schemes. The difference is that F_{pmci} represents the two different magnetomotive forces of the main and auxiliary PMRs. The main magnetic flux Φ_m is generated by two parts, trapezoidal PMR and auxiliary PMR. Furthermore, the two

trapezoidal PMRs and two auxiliary PMRs are the same, respectively. The corresponding magnetic reluctances are R_{pmc1} and R_{pmc2} , and the corresponding magnetization lengths are l_{pmc1} and l_{pmc2} , respectively. The magnetic flux density B can be expressed as

$$B = \text{diag}(A_{\sigma u}, A_u, A_{\sigma c}, A_c)^{-1} \begin{bmatrix} R_u / (R_{\sigma u} + R_u) \\ R_{\sigma u} / (R_{\sigma u} + R_u) \\ R_c / (R_{\sigma c} + R_c) \\ R_{\sigma c} / (R_{\sigma c} + R_c) \end{bmatrix} \cdot \frac{2(H_c l_{\text{pmc1}} + H_c l_{\text{pmc2}})}{2(R_{\text{pmc1}} + R_{\text{pmc2}}) + \frac{R_u R_{\sigma u}}{R_u + R_{\sigma u}} + \frac{R_c R_{\sigma c}}{R_c + R_{\sigma c}}} \quad (8)$$

It can be seen from Fig.7(a) that the magnetic flux densities at lower end region of upper winding and upper end region of lower winding are reduced. The reason is that the leakage magnetic flux around air gap side does not flow through the coil. In implicit trapezoid double magnetic circuits LFTMB scheme, the auxiliary and main magnetic fluxes are superimposed at winding region. The magnetic circuit superposition can effectively improve

the magnetic flux shown in the transition region in Fig.10(a) and transition region in orange in Fig.10(b). In addition, the magnetic flux leakage of the rectangular PMR is also compensated by the increased magnetization length of the trapezoidal PMR, which causes the magnetic flux density in the interface between the winding and transition regions decreased. It is shown in orange in Fig.10(b).

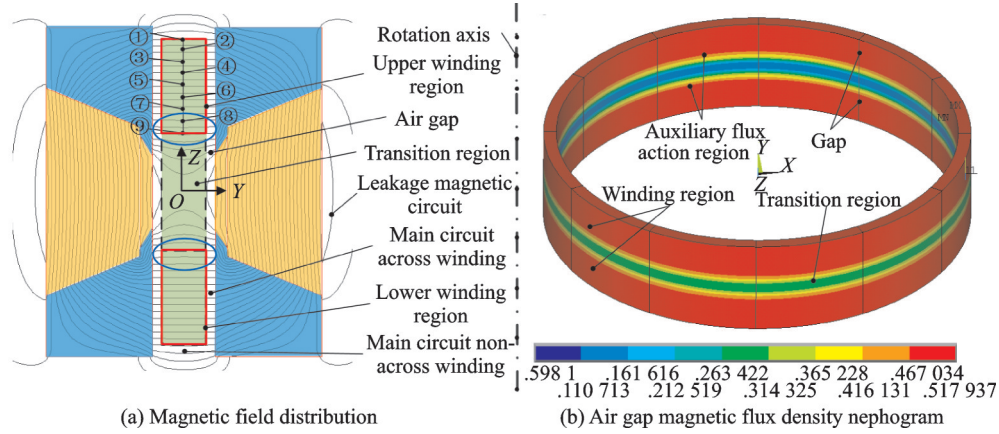


Fig.10 Implicit trapezoid double magnetic circuits LFTMB

The magnetic flux density of implicit trapezoid double magnetic circuits LFTMB is related to the magnetization length according to Eq.(1). In order to obtain the optimal LFTMB, the magnetization

length is analyzed. As shown in Fig.11, the relationship curves between magnetic flux density and longitudinal length of magnetic pole are plotted. As can be seen from Fig.11 that when the longitudinal

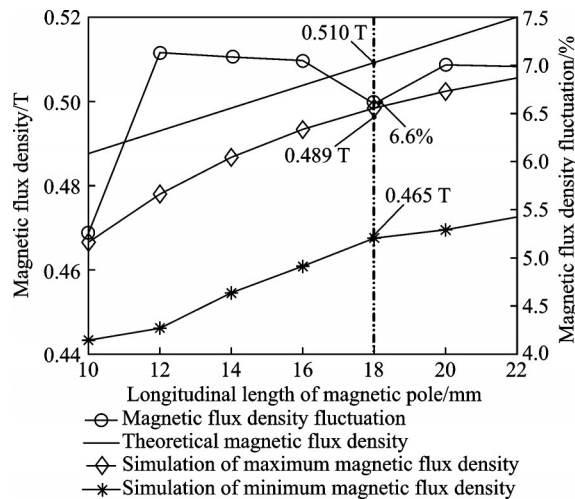


Fig.11 Longitudinal length of magnetic pole versus magnetic flux density and magnetic flux density fluctuation

length of magnetic pole is 18 mm, the magnetic flux density of 0.489 T and the corresponding fluctuation of 6.6% is better than others. The corresponding theoretical magnetic flux density is 0.510 T, and the error between the theoretical analysis and simulation is within 5%, indicating the consistency between the theoretical analysis and simulation.

Based on the optimal longitudinal length of magnetic pole of 18 mm, the design parameters are shown in Table 1. According to Table 1, the magnetic flux density distribution along the radial direction of implicit trapezoid double magnetic circuits LFTMB is shown in Fig.12(a). The maximum and minimum magnetic flux densities are 0.498 T and 0.465 T, respectively, both of which are larger than those of implicit single magnetic circuit LFTMB with 0.428 T and 0.397 T. The corresponding magnetic flux density fluctuation with 6.6% is improved a little compared with that of implicit single magnetic circuit LFTMB. Circumferential magnetic flux density distribution is shown in Fig.12(b). The maximum and minimum magnetic flux densities are 0.489 T in the 5th line and 0.469 T in the 9th line, respectively. Its circumferential magnetic flux densi-

ty fluctuation is 4.0%, which is better than that of implicit single magnetic circuit LFTMB. Whether it is radial magnetic flux density fluctuation or circumferential magnetic flux density fluctuation, the implicit trapezoid double magnetic circuits LFTMB has significant improvement over implicit single magnetic circuit LFTMB.

Table 1 Design results of the implicit trapezoid double magnetic circuits LFTMB

| Parameter | Value/mm |
|--|----------|
| Outer cylinder radius of the outer magnetic ring | 70 |
| Inner cylinder radius of the outer magnetic ring | 61.5 |
| Outer cylinder radius of the inner magnetic ring | 56.9 |
| Inner cylinder radius of the inner magnetic ring | 48.2 |
| Upper length of main trapezoid PMR | 10 |
| Bottom length of main trapezoid PMR | 18 |
| Main trapezoid PMRs wall thickness | 7.5 |
| Auxiliary trapezoid PMRs wall thickness | 1.2 |
| Upper length of auxiliary trapezoid PMR | 6 |
| Bottom length of auxiliary trapezoid PMR | 9 |
| Longitudinal length of magnetic pole | 18 |
| Section height of the winding | 8 |
| Section thickness of the winding | 3.4 |
| Wire diameter of the winding | 0.25 |
| Air gap length | 4.6 |

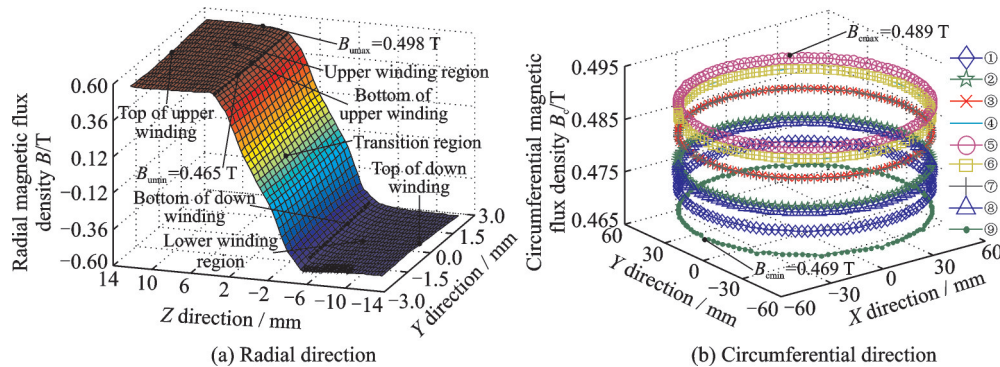


Fig.12 Magnetic flux density distribution

2 LFTMB Schemes Contrastive Analysis

The magnetic flux densities of the three schemes are obtained by variance calculation, and the three fluctuation variance curves are shown in Fig.13. Taken for calculation and the up winding region is taken as an example, the curves of radial fluctuation variance are plotted in Fig.13(a) when

the coil effective region is considered. Due to the magnetic flux leakage at the upper and lower end regions of the winding, the fluctuation is large at the end region, and the intermediate magnetic flux densities are relatively uniform. So the curve is in the shape of a parabola with an open upward. It can be visually seen from Fig.13(a) that the radial fluctuation variance of implicit trapezoid double magnetic circuits LFTMB is the smallest and the magnetic

flux density is the most uniform. The three curves of circumferential fluctuation variance are shown in Fig.13(b), which shows that the circumferential fluctuation variances of the three schemes are 4.96%, 1.03% and 0.66%, respectively. Based on the contrastive analysis of magnetic flux density fluctuation, the implicit trapezoid double magnetic circuits LFTMB is optimal to adopt.

3 Experiment

As shown in Fig.14, an implicit double magnetic circuits LFTMB prototype is manufactured. The LFTMB is placed in the edge groove of gyrowheel rotor. The design parameters of LFTMB are listed in Table 1. The section thickness and width of upper or lower winding are 8 mm and 3.4 mm, respectively. The experimental setup is shown in Fig.14. The gyrowheel rotor is fixed on the rotary table, which is driven to rotate by step motor. A Hall sensor located in the air gap is used for measuring the air gap magnetic flux density of LFTMB. The whole magnetic

flux density in the whole winding region is obtained. The magnetic flux density testing results in the radial and circumferential directions are shown in Fig.15. It can be clearly seen from Fig.15(a) that the maximum and minimum magnetic flux densities in the radial direction are 0.492 T and 0.453 T, respectively. Its circumferential magnetic flux density fluctuation is 7.9%. The difference between experimental and theoretical values of radial magnetic flux density is 1.5%. As shown in Fig.15(b), the maximum and minimum values of magnetic flux density are 0.485 T and 0.458 T, respectively. The circumferential magnetic flux density fluctuation is 5.5%. The difference between experimental and theoretical values of circumferential magnetic flux density is 1.5%. Due to the decrease of magnetic motive force of permanent magnetic rings during the process of manufacture, the experimental values of magnetic flux density are less than theoretical values, and experimental values of magnetic flux density fluctuation are a little larger than testing values.

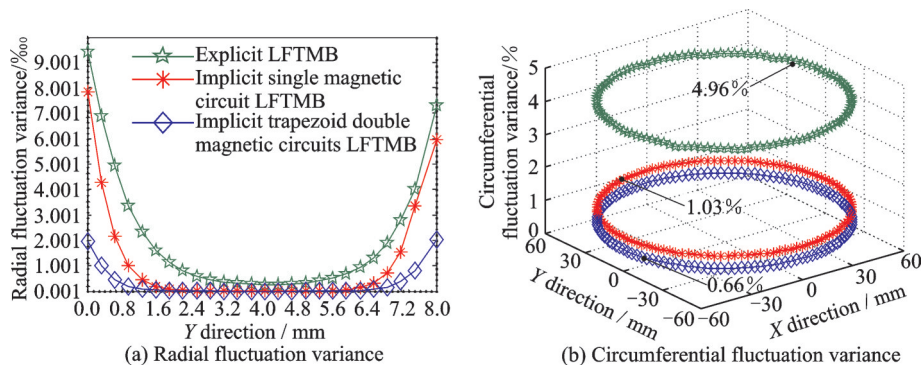


Fig.13 Contrastive curve of three schemes

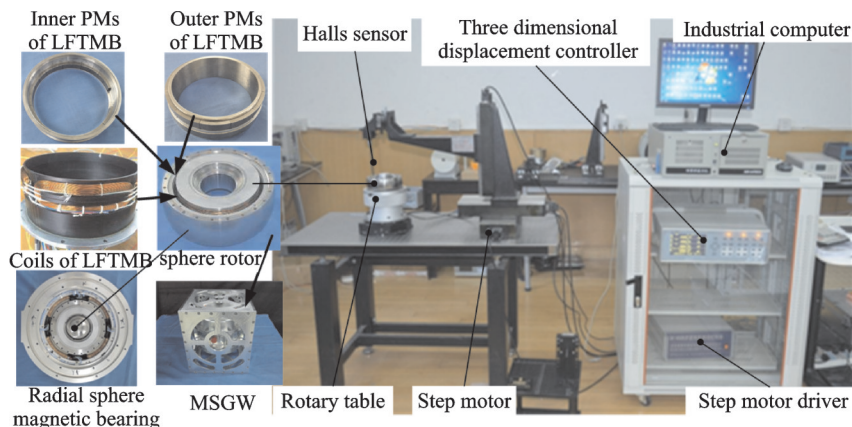


Fig.14 Magnetic flux density experiment system

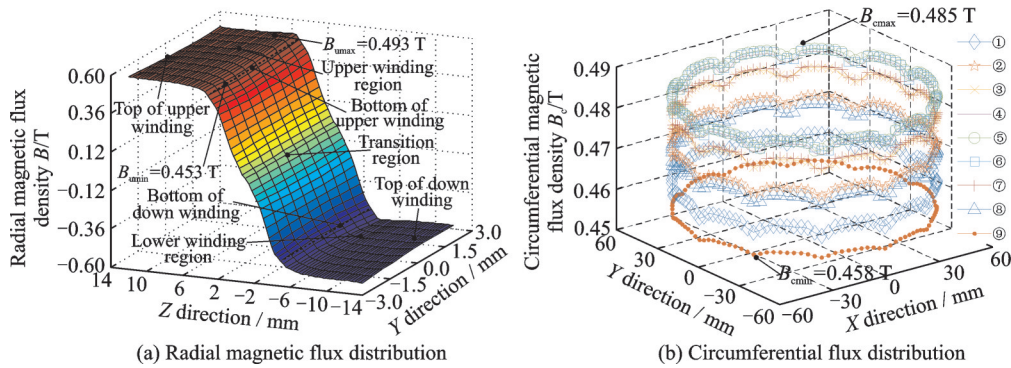


Fig.15 Magnetic flux density test results of implicit double magnetic circuits LFTMB

4 Conclusions

To remedy the limitation of conventional explicit LFTMBs with poor magnetic flux density, two implicit LFTMB schemes are proposed. The LFTMB deflection model is established, and the deflection torque precision is proven to be related to the magnetic flux density uniformity. By building the finite element model, the radial magnetic flux density fluctuations of the three LFTMB schemes are obtained as 25%, 7.2% and 6.6%. And the circumferential flux density fluctuation of that are 26%, 5.2% and 4.0%. By contrastive analysis, the implicit trapezoid double magnetic circuits LFTMB scheme is adopted for MSGW to provide high-precision deflection torque. The test result shows that the maximum and the minimum circumferential magnetic flux densities are 0.485 T and 0.458 T, respectively. Its circumferential magnetic flux density fluctuation is 5.5%. It is verified by the theoretical analysis and the prototyped experiments that the difference between the theoretical value and the experimental value of circumferential magnetic flux density is 1.5%. This indicates that the implicit double magnetic circuits LFTMB and the theoretical analysis is effective and valid. Moreover, the scheme is competent to meet the requirements for high precision control of MSGW.

References

- [1] KOJIMA H, TRIVAILO P M. Adaptive time-delay estimated sliding mode control for a bias momentum satellite with two reaction wheels[J]. Transactions of the Japan Society for Aeronautical and Space Scienc-
- es, 2019, 62(4):236-245.
- [2] HUTTERER M, GERALD KALTEIS M S. Redundant unbalance compensation of an active magnetic bearing system[J]. Mechanical Systems and Signal Processing, 2017, 94:267-278.
- [3] JIAN F, KUN L, JINGBO W. Instantaneous torque control of magnetically suspended reaction flywheel[J]. Energy Procedia, 2016, 100:297-306.
- [4] PENG C, FANG J, WANG C. Steering law for a cluster of magnetically suspended momentum wheels with vernier gimbaling capability[J]. International Journal of Applied Electromagnetics & Mechanics, 2015, 47(3):691-704.
- [5] DAGNAES-HANSEN N A, SANTOS I F. Magnetically suspended flywheel in gimbal mount—Nonlinear modelling and simulation[J]. Journal of Sound & Vibration, 2018, 432:327-350.
- [6] SUN J J, JU Z, PENG C, et al. A novel 4-DOF hybrid magnetic bearing for DGMSCMG[J]. IEEE Transactions on Industrial Electronics, 2017, 64(3): 2196-2204.
- [7] MURAKAMI C, OHKAMI Y, OKAMOTO O, et al. A new type of magnetic gimballed momentum wheel and its application to attitude control in space[J]. Acta Astronautica, 1984, 11(9):613-619.
- [8] SEDDON J, PECHEV A. 3-D wheel: A single actuator providing three-axis control of satellites[J]. Journal of Spacecraft and Rockets, 2013, 49(3):553-556.
- [9] TANG J Q, SUN J J, FANG J C, et al. Low eddy loss axial hybrid magnetic bearing with gimbaling control ability for momentum flywheel[J]. Journal of Magnetism and Magnetic Materials, 2013, 329(2): 153-164.
- [10] GERLACH B, EHINGER M, RAUE H K, et al. Digital controller for a gimbaling magnetic bearing reaction wheel[J]. AIAA Journal, 2005, 8:6244-6249.

- [11] LI J, XIAO K, LIU K, et al. Mathematical model of a vernier gimbaling momentum wheel supported by magnetic bearings[C]//Proceedings of the 13th International Symposium on Magnetic Bearings. Changsha: [s.n.], 2012: 1-9.
- [12] XIANG B, TANG J. Suspension and titling of vernier-gimbaling magnetically suspended flywheel with conical magnetic bearing and Lorentz magnetic bearing[J]. *Mechatronics*, 2015, 28:46-54.
- [13] TANG J Q, XIANG B, WANG C. Rotors suspension for Vernier-gimbaling magnetically suspended flywheel with conical magnetic bearing[J]. *ISA Transactions*, 2015, 58:509-519.
- [14] DAMIEN C, CHRISTIAN C, JÉRÔME D, et al. Magnetic centering bearing with high-amplitude tilt control: U.S. Patent 6 384 500[P]. 2002-05-07.
- [15] LIU Q, LI H, WANG W, et al. Analysis and experiment of 5-DOF decoupled spherical vernier-gimbaling magnetically suspended flywheel (VGMSFW)[J]. *IEEE Access*, 2020(8):111707-111717.

Acknowledgements This work was supported by Beijing Municipal Natural Science Foundation (General Program) (No. 3212004) and Cultivation Project of Important Scientific Research Achievements of Beijing Institute of Petrochemical Technology (No. BIPTACF-007).

Author Ms. WANG Qirui received her B.S. degree in Electronic and Information Engineering from Anhui Normal University in 2018 and M.S. degree in Mechanical Engineering from Beijing Institute of Petrochemical Technology in 2021. Her research interests include the design and optimization of Lorentz force-type magnetic bearing.

Author contributions Ms. WANG Qirui contributed to the conceptualization, methodology, experiment, data curation and formal analysis of the manuscript. Prof. LIU Qiang contributed to the funding acquisition, conceptualization, visualization and the supervision. Mr. LI Zhuang contributed to the experiment, software and data curation. All authors commented on the manuscript draft and approved submission.

Competing interests The authors declare no competing interests.

(Production Editor: WANG Jing)

高精度敏捷机动磁悬浮陀螺飞轮用新型隐式洛伦兹磁轴承

王琪瑞, 刘强, 李状

(北京石油化工学院机械工程学院, 北京 102617, 中国)

摘要: 具有良好线性的洛伦兹力型磁轴承适用于磁悬浮陀螺的高精度偏转控制。针对现有显式洛伦兹力型磁轴承磁通密度均匀性差的问题, 本文提出了两种可以提高磁通密度均匀性新型隐式洛伦兹力磁轴承。介绍了3种洛伦兹力磁轴承的结构, 基于等效磁路法建立了其数学模型, 并采用有限元法对磁场进行了分析。仿真结果表明, 隐式洛伦兹力型磁轴承的磁通密度均匀性优于传统显式洛伦兹力型磁轴承。此外, 双磁路隐式梯形洛伦兹力磁轴承在磁通密度均匀性和磁通密度方面优于单磁路隐式洛伦兹力型磁轴承。本文进一步对双磁路隐式梯形洛伦兹力磁轴承的磁通密度进行实验验证, 实验结果与仿真结果误差不超过5%, 说明双磁路隐式梯形洛伦兹力磁轴承可以满足磁悬浮陀螺高精度敏捷机动的要求。

关键词: 有限元法; 洛伦兹力磁轴承; 磁悬浮陀螺飞轮; 磁通密度均匀性